J Solid State Electrochem (2009) 13:905–912
DOI 10.1007/s10008-008-0627-y

ORIGINAL PAPER

# Study of capacitive properties for LT-$Li_4Mn_5O_{12}$ in hybrid supercapacitor

**Yan-Jing Hao · Yan-Ying Wang · Qiong-Yu Lai · Yan Zhao · Lian-Mei Chen · Xiao-Yang Ji**

Received: 11 June 2008 / Revised: 30 June 2008 / Accepted: 7 July 2008 / Published online: 29 July 2008


**Abstract** Spinel $Li_4Mn_5O_{12}$ nanoparticles have been prepared by a very simple sol–gel method. Various initial conditions were studied in order to find the optimal conditions for the synthesis of pure $Li_4Mn_5O_{12}$. X-ray diffraction results showed that spinel $Li_4Mn_5O_{12}$ was obtained at a low temperature of 300 °C without any miscellaneous phase. Scanning electron microscope analyses indicated that the prepared $Li_4Mn_5O_{12}$ powders had a uniform morphology with average particle size of about 50 and 100 nm. The prepared sample was firstly used as a cathode material in an asymmetric $Li_4Mn_5O_{12}$/AC supercapacitor in aqueous electrolyte. The capacitive properties of the hybrid supercapacitor were tested by cyclic voltammetry, electrochemical impedance spectroscopy, and galvanostatic charge–discharge tests. The results showed that $Li_4Mn_5O_{12}$ annealed at 450 °C for 4 h exhibited the best electrochemical capacitive performance within the potential range of 0–1.4 V in 1 M $Li_2SO_4$ solution. A maximum specific capacitance of 43 F $g^{-1}$ based on the total active material weight of the two electrodes was obtained for the $Li_4Mn_5O_{12}$/AC supercapacitor at a current density of 100 mA $g^{-1}$. The capacitor showed excellent cycling performance and structure stability via 1,000 cycles.

**Keywords** Spinel $Li_4Mn_5O_{12}$ · Capacitive properties · Hybrid supercapacitor · Aqueous electrolyte

Y.-J. Hao · Y.-Y. Wang · Q.-Y. Lai (✉) · Y. Zhao · L.-M. Chen
College of Chemistry, Sichuan University,
Chengdu 610064, China
e-mail: Laiqy5@hotmail.com

X.-Y. Ji
Analyzing and Testing Center, Sichuan University,
Chengdu 610064, China

## Introduction

In recent years, many research works have been done in electrochemical capacitors aiming to increase power and energy density as well as reduce fabrication costs while using environmental friendly materials simultaneously. Electrochemical capacitors coupled with batteries are considered promising solutions providing the power peaks for acceleration and regenerative braking and recovering the breaking energy for electric vehicle (EV). Developing a hybrid system that consists of a double-layer capacitor (EDLC) electrode and a battery electrode was an effective way. For the hybrid supercapacitor, one electrode stores charge through a reversible non-faradaic reaction of ion adsorption/desorption on the surface of AC material and the other electrode utilizes a reversible redox faradaic reaction in a lithium-ion intercalated compound. In hybrid systems, the electrolyte works in the similar way to the EDLCs. The increasing of the working voltage and the high energy density of the battery electrode material in hybrid capacitors result in a significant increase in the energy density of the capacitors compared with that of EDLCs. Some lithium-ion intercalated materials such as $Li_2Ti_3O_7$, $Li_4Ti_5O_{12}$, and $LiCoO_2$ have been used as the electrode materials of hybrid supercapacitor in organic electrolyte [1–4] and $LiMn_2O_4$, $LiNi_{1/3}Co_{1/3}Mn_{1/3}O_2$, and $LiCoO_2$ in aqueous solution [5–7]. These hybrid pseudocapacitors show higher energy density, long cycle life, and fast charge–discharge rate.

Among all of the lithium-ion battery materials, spinel-type electrodes are becoming the promising electrode materials in terms of the intercalation potential, cyclability, and rate capability for the development of polymer lithium-ion batteries and hybrid supercapacitors [8–11]. The $[M_2]O_4$ framework of a $Li[M_2]O_4$ spinel is an attractive host structure for lithium insertion–extraction reactions because

it provides a three-dimensional network of face-sharing tetrahedra and octahedra for lithium-ion diffusion.

The spinel-type lithium manganese oxides, which were seen as potentially low cost and environmentally benign electrode materials, have been examined extensively in recent years. Among them, the spinel $LiMn_2O_4$ has become of particular interest in the past decade [12–17]. However, large capacity fade on cycling is encountered in the 3 V region due to Jahn–Teller distortion as the average valence of manganese falls below +3.5 in $LiMn_2O_4$ [14, 18]. $Li_4Mn_5O_{12}$ is a stoichiometric spinel with cubic symmetry and cationic arrangement Li $[Li_{0.33}Mn_{1.67}]$ $O_4$. With a manganese oxidation state of +4, the Jahn–Teller distortion, which causes the capacity fading of the spinel $LiMn_2O_4$ on cycling, can be suppressed in $Li_4Mn_5O_{12}$ [19].

Furthermore, preparation of $LiMn_2O_4$ needs high calcinations temperature (about 800 °C) and long heated time (about 12~24 h) [20]. So people called it high-temperature spinel $LiMn_2O_4$ (HT-$LiMn_2O_4$). Compared with that of $LiMn_2O_4$, $Li_4Mn_5O_{12}$ is conventionally synthesized at lower temperature (about 450 °C) and for shorter calcination times (about 4~6 h) [21]. So people called it low-temperature spinel $Li_4Mn_5O_{12}$ (LT-$Li_4Mn_5O_{12}$).

In this work, LT-$Li_4Mn_5O_{12}$ was prepared by a simple sol–gel method with citric acid as chelating agent at a very low temperature of 300 °C. The pseudocapacitive properties of $Li_4Mn_5O_{12}$ were firstly examined in electrochemical capacitor $Li_4Mn_5O_{12}$/AC in which $Li_4Mn_5O_{12}$ was used as the cathode material and activated carbon (AC) was used as the anode material. The combination of $Li_4Mn_5O_{12}$ and AC within aqueous electrolyte provides good cycle life and the use of aqueous electrolyte can overcome the drawbacks of safety hazards from the use of highly toxic and flammable organic solvents.

## Experimental

### Preparation of $Li_4Mn_5O_{12}$

$Li_4Mn_5O_{12}$ was prepared by a sol–gel process with $LiAc{\cdot}2H_2O$ (AR, 99%) and $MnAc_2{\cdot}4H_2O$ (AR, 99%) used as starting materials. All the chemicals were provided by Chengdu KeLong Industries Co., China. Required amounts of the raw materials with the molar ratio of Li:Mn=4:5 were dissolved in appropriate distilled water and stirred. The aqueous solution of citric acid was added to the mixed solution under stirring to obtain a crystal clear solution; the ratio of citric acid to total metal ions was 1:1. And then, ammonia solution was dropped until pH value of the admixture solution was about 8–9 to obtain a sol. The clear sol was continued to be heated and stirred until water was removed from the sol and then a viscous gel was obtained. The resulting gel was dried at 100 °C over 6 h to extract excess water and yield organic precursors. The gel precursors were preheated at 300 °C for 2 h in air and then calcined at 250, 300, 450, 600, and 700 °C for 4 h in air, respectively.

Activated carbon (AC) was provided by the Research Institute of Chemical Defense—Beijing, China.

### Characterization of $Li_4Mn_5O_{12}$

The samples were characterized by X-ray diffraction (XRD), using a D/max-rA diffractometer with Cu Kα radiation operated at 40 kV and 100 mA. Data were collected in the range 10–70° ($\lambda$=0.15418 nm). The scanning electron microscope (SEM, Hitachi-S-450, Japan) was used to observe the morphology and size of prepared particles.

### Measurement of electrochemical properties

The cathode electrode was prepared by mixing 75 wt.% of the $Li_4Mn_5O_{12}$ with 20 wt.% acetylene black and 5 wt.% polyvinylidene fluoride (PVDF) using *N*-methy1–2-pyrrolidine as the solvent. After the mixture was sufficiently blended, the obtained slurry was subsequently brush-coated on to a stainless steel grid and then dried to obtain the $Li_4Mn_5O_{12}$ electrode. Preparation of AC anode electrode was similar to that of $Li_4Mn_5O_{12}$ electrode. The AC anode electrode contained 65 wt.% AC, 5 wt.% PVDF, and 30 wt.% acetylene black. The fabricated hybrid supercapacitors were tested in different aqueous electrolytes (1 mol $l^{-1}$ $Li_2SO_4$, 1 mol $l^{-1}$ $(NH_4)_2SO_4$, 1 mol $l^{-1}$ $Na_2SO_4$, 1 mol $l^{-1}$ $K_2SO_4$) at different current densities (100–400 mA $g^{-1}$) in the range of 0–1.4 V at room temperature by Neware Battery Program Control Test System.

The cyclic voltammetry was characterized by using a three-electrode cell, in which a stainless steel grid coated with $Li_4Mn_5O_{12}$ was used as the working electrode and platinum and saturated calomel electrode (SCE, 0.242 V) as the counter and reference electrode, respectively. The measurements were performed on an LK2005 electrochemical workstation system.

The electrochemical impedance spectroscopy experiment was also carried out by using a three-electrode cell, and it was performed by using Potentiostat/Galvanostat IM6ex (ZHANER Elektrik; Germany) instrument. The frequency limits were typically set between 1000 kHz and 0.01 Hz.

## Results and discussions

### XRD analysis

Figure 1 showed the powder X-ray diffraction patterns of $Li_4Mn_5O_{12}$ prepared at 250, 300, 450, 600, and 700 °C for

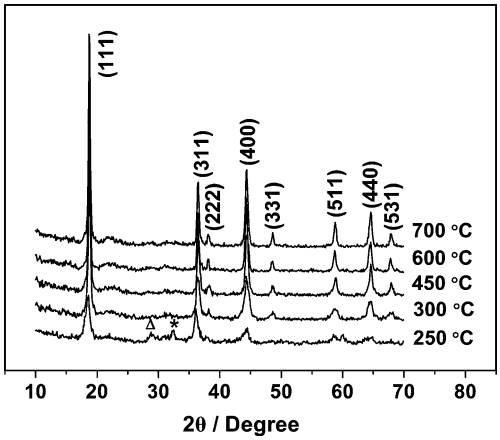


**Fig. 1** X-ray diffraction patterns of $Li_4Mn_5O_{12}$ prepared at different temperatures. Δ $MnO_2$; * $Mn_2O_3$

4 h in air. The results indicated that the sample obtained at 250 °C contained $MnO_2$ and $Mn_2O_3$ miscellaneous phase. When heating temperature was increased to above 300 °C, all the XRD patterns are in agreement with JCPDS card no. 46-0810. The cubic lattice parameter of $Li_4Mn_5O_{12}$ at 300, 450, and 600 °C was calculated to be $a$=8.1705 Å, $a$= 8.1677 Å, and $a$=8.1799 Å. These results were very close to JCPDS card no. 46-0810 ($a$=8.161 Å) and in good agreement with those obtained by C. M. Julien et al. [9] and Toshimi Takada et al. [22]. The results indicated that all samples are spinel $Li_4Mn_5O_{12}$ single phase.

As can be seen in Fig. 1, the diffraction peaks of $Li_4Mn_5O_{12}$ gradually sharpened with the increasing of temperature, which indicates an increase of crystallinity as may occur from the growth of grain size and ordering of local structure. All the diffraction peaks can be indexed based on a face-centered cubic spinel structure with *Fd*3*m* space group, where lithium ions are located at the tetrahedral 8a sites, and tetravalent manganese ions and lithium ions are randomly distributed at octahedral 16d sites by the ratio of Li/Mn=1:5, while oxygen ions are located at the 32e sites. Thus, $Li_4Mn_5O_{12}$ can be described as $[Li]_{8a}[Li_{1/3}Mn_{5/3}]_{16d}[O_4]_{32e}$ [23].

## SEM analysis

The SEM images of $Li_4Mn_5O_{12}$ powders prepared at 300, 450, and 600 °C for 4 h are shown in Fig. 2. As can be seen in the figure, powders heated at 300 and 450 °C for 4 h were composed of some irregular analogue globular nanoparticles. The average particle sizes were about 50 nm and 100 nm, respectively. When temperature increased to 600 °C, the average particles size of $Li_4Mn_5O_{12}$ sample increased obviously. This indicated that the soft-chemistry method and the lower annealing temperature are favorable for forming a product with smaller particle size, which are favorable for improving pseudocapacitance properties of $Li_4Mn_5O_{12}$.

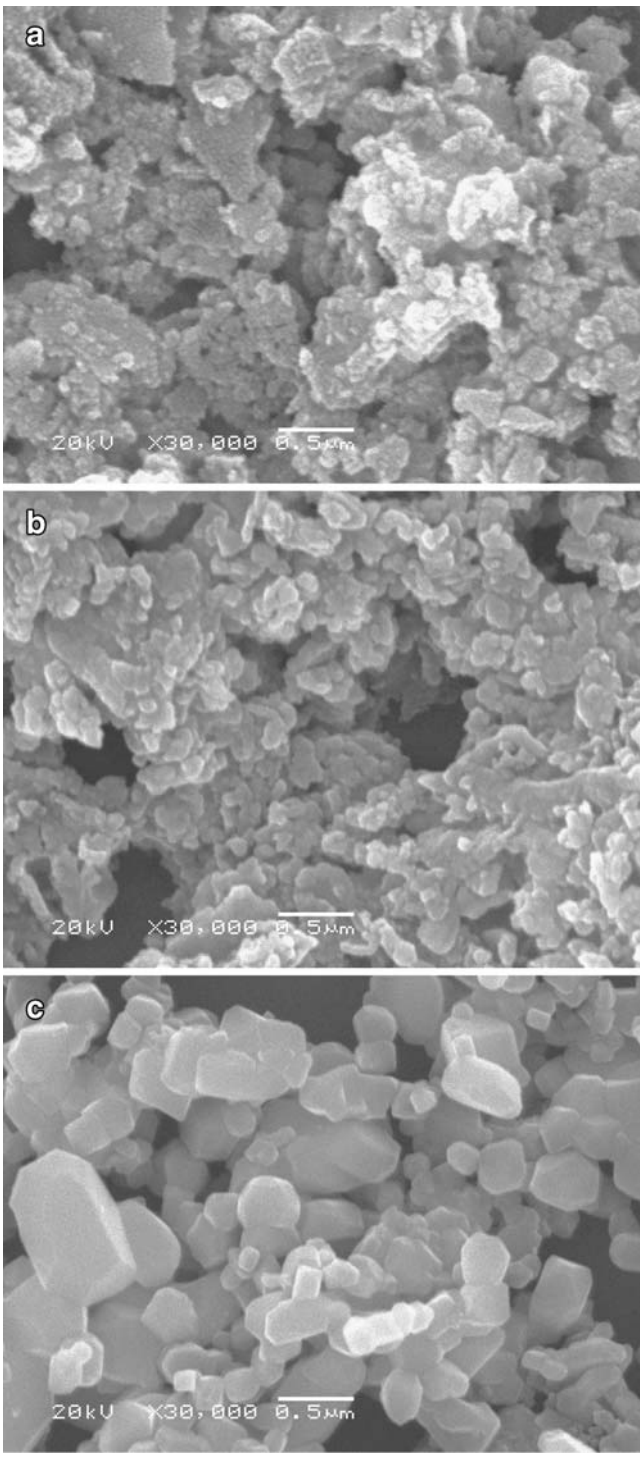


**Fig. 2** SEM photograph of $Li_4Mn_5O_{12}$ prepared at 300, 450, and 600 °C for 4 h. **a** 300 °C, **b** 450 °C, **c** 600 °C

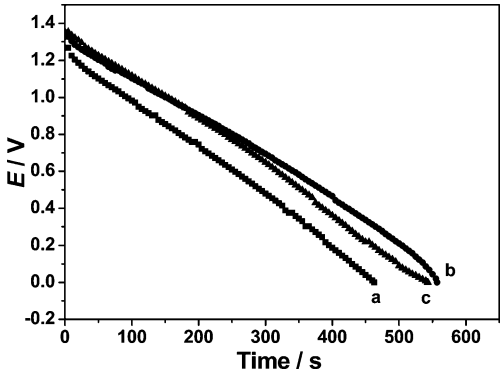


**Fig. 3** Typical discharge curves of $Li_4Mn_5O_{12}$/AC hybrid pseudocapacitor with $Li_4Mn_5O_{12}$ prepared at different temperature. **a** 300°C, **b** 450°C, **c** 600°C

## Electrochemical performance

### *Electrochemical performance of $Li_4Mn_5O_{12}$ prepared at different temperatures*

Figure 3 shows the 20th cycle discharge curve of $Li_4Mn_5O_{12}$ 1 M $Li_2SO_4$/AC hybrid aqueous pseudocapacitor at a current rate of 100 mA $g^{-1}$ between 0 and 1.4 V. $Li_4Mn_5O_{12}$ sample was prepared at different annealing temperatures of 300, 450, and 600 °C for 4 h in air, respectively. As shown, a good linear variation of potential versus time was observed for both curves, which is a typical characteristic of an ideal supercapacitor. Based on the discharge curves, the discharge specific capacity ($C_s$) of the hybrid pseudocapacitors were calculated as the following formula:

$$C_s = \frac{i \times \Delta t}{m \times \Delta V} \quad (1)$$

Where $i$ is the current of charge–discharge, $\Delta t$ is the time of discharge, $\Delta V$ is the discharge voltage difference, and $m$ is the mass of active materials based on the total weight of positive electrode and negative electrode within the capacitor.

According to the above equation, specific capacitances of hybrid capacitor based on $Li_4Mn_5O_{12}$ material calcined at 300, 450, and 600 °C were calculated to be 40, 43, and 42 F $g^{-1}$, respectively. Cycling performance of the hybrid supercapacitor with $Li_4Mn_5O_{12}$ materials calcined at 300, 450, and 600 °C are shown in Fig. 4. As can be seen in Fig. 4a and c, the hybrid supercapacitors exhibited poor cycling life. After 200 cycles, the specific capacitance of the two capacitors decreased to 30 and 35 F $g^{-1}$, respectively. While in Fig. 4b, the hybrid pseudocapacitor showed a good cycle performance with the specific capacitance remained 39 F $g^{-1}$ after 200 cycles. The above results indicated that the hybrid supercapacitor fabricated with spinel $Li_4Mn_5O_{12}$ heated at 450 °C showed the best electrochemical properties in 1 M $Li_2SO_4$ aqueous electrolyte.

According to the results obtained from the SEM and XRD, the sample synthesized at 450 °C had the smaller particles and relatively high crystallinity; it also had the better electrochemical properties. For $Li_4Mn_5O_{12}$/1 M $Li_2SO_4$/AC hybrid supercapacitor, the AC electrode stores charge through a reversible non-faradaic reaction of ion adsorption/desorption on the surface of the material, and the lithium-ion intercalated $Li_4Mn_5O_{12}$ electrode material utilizes a reversible redox faradaic reaction. So in hybrid systems, the particle size and morphology of lithium-ion intercalated $Li_4Mn_5O_{12}$ materials have a definite effect on the electrochemical properties of supercapacitors. According to A. Singhal et al. [24], smaller particles have shorter diffusion distances for intercalated Li-ion materials. C. M. Julien et al. [9] reported that the decrease in the particle size of $Li_{4/3}Ti_{5/3}O_4$ spinels is unequivocally correlated with kinetics of grain formation using the proposed HEBM synthesis, which favors the tendency of small grains, since electrochemical lithium intercalation and deintercalation are in general limited by the rate of diffusion. The aforementioned features are important since smaller grain size can favor the lithium-ion mobility in the particles by reducing the ion-diffusion pathway. In our case, the $Li_4Mn_5O_{12}$ material had the similar characteristics. So samples that had smaller particle size had the better performance. For this reason, in all latter studies, $Li_4Mn_5O_{12}$ samples annealed at 450 °C for 4 h was chosen for the cathode of $Li_4Mn_5O_{12}$/AC hybrid pseudocapacitor.

Cycling stability of the $Li_4Mn_5O_{12}$/AC hybrid aqueous pseudocapacitors was examined by means of charge–discharge tests in a potential range of 0–1.4 V at a current rate of 100 mA $g^{-1}$. As indicated in Fig. 5, $Li_4Mn_5O_{12}$/AC pseudocapacitor exhibits good cycling performance with

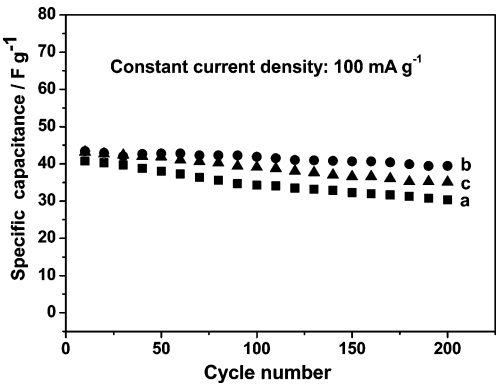


**Fig. 4** Cycling profiles of the $Li_4Mn_5O_{12}$/1 M $Li_2SO_4$/AC hybrid pseudocapacitor with $Li_4Mn_5O_{12}$ prepared at different temperatures at a current rate of 100 mA $g^{-1}$. **a** 300 °C; **b** 450 °C, **c** 600 °C

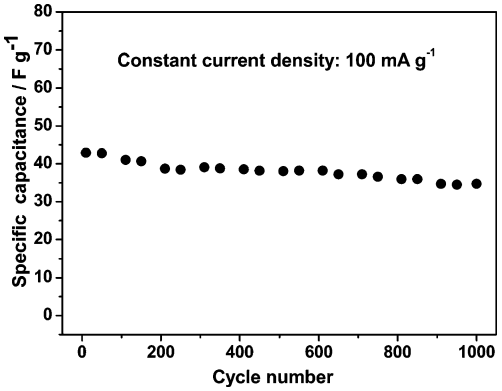


**Fig. 5** Cycling stability of $Li_4Mn_5O_{12}$/AC hybrid aqueous capacitor at a current rate of 100 mA $g^{-1}$

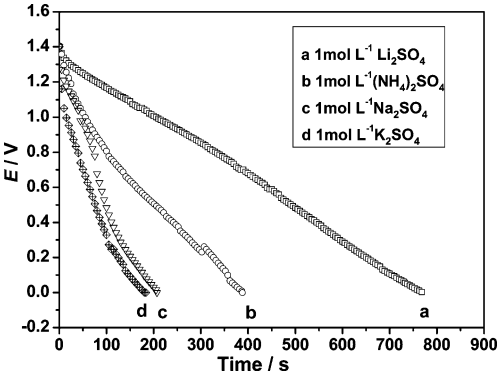


**Fig. 7** Typical discharge curves of $Li_4Mn_5O_{12}$/AC hybrid pseudocapacitor in different electrolyte

the capacity fading rate of only 0.0078 F $g^{-1}$ per cycle after 1,000 cycles.

The structure of $Li_4Mn_5O_{12}$ prepared at 450 °C before and after 50th cycle is analyzed by XRD. The typical XRD patterns of $Li_4Mn_5O_{12}$ before charge–discharge cycles and after 50th cycle are given in Fig. 6. It can clearly be seen that the sample after 50th cycle still remained as single-phase spinel $Li_4Mn_5O_{12}$, indicating that the lattice structure of $Li_4Mn_5O_{12}$ prepared at 450 °C was stable when Li-ions are rapidly inserted and extracted.

*Effect of different electrolytes*

The influence of various aqueous solutions on the capacitive behavior of supercapacitor was investigated in order to find the most appropriate electrolyte. Figure 7 shows the typical discharge curves of $Li_4Mn_5O_{12}$/AC measured in 1 M $Li_2SO_4$, 1 M $(NH_4)_2SO_4$, 1 M $Na_2SO_4$, and 1 M $K_2SO_4$ solutions between 0 and 1.4 V at a scan rate of 100 mA $g^{-1}$.

The results indicated that the $Li_4Mn_5O_{12}$/AC capacitor exhibited the best electrochemical performance in 1 M $Li_2SO_4$ solution than in other aqueous electrolytes, which indicates that the species and size of the cation such as $Li^+$, $Na^+$, $NH_4^+$, and $K^+$ in the systems had definite influence on the electrochemical performance of supercapacitor. The data also showed that the charge storage mechanism of the $Li_4Mn_5O_{12}$ cathode material in the potential range of 0–1.4 V in aqueous electrolyte is associated with the insertion/deinsertion of Li-ion, which is similar to the charge storage mechanism of $Li_4Mn_5O_{12}$ material in organic electrolyte.

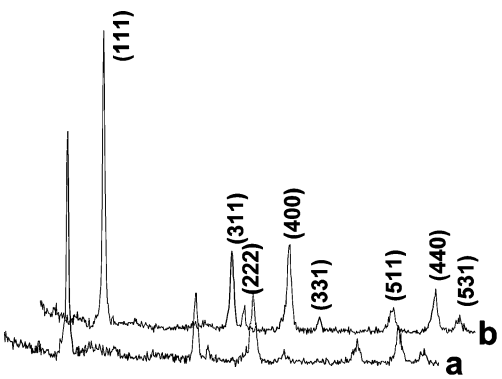


**Fig. 6** XRD patterns of the $Li_4Mn_5O_{12}$. **a** After 100th cycling in 1 M $Li_2SO_4$ at a current rate of 100 mA $g^{-1}$; **b** before cycling

The structure of the spinel $Li_4Mn_5O_{12}$ could easily accommodate to insert $Li^+$ ions. During discharge process, Li-ions first intercalate into 16c sites in $Li_4Mn_5O_{12}$ structure, and then into the tetrahedral 8a sites, which also migrate to 16c sites. Eventually, the 16c sites are occupied by Li-ions. As demonstrated above, there is the mechanism proposed for the charge–discharge storage in $Li_4Mn_5O_{12}$ electrode, which is based on the concept of intercalation of $Li^+$ ions [25]. It can be described as follows:

$$Li_{4+x}Mn_5O_{12} \underset{\text{Discharge}}{\overset{\text{Charge}}{\rightleftharpoons}} Li_4Mn_5O_{12} + xLi^+ + xe^-$$

During the charge process, Li-ions in spinel $Li_{4+x}Mn_5O_{12}$ material were easily deinserted to form $Li_4Mn_5O_{12}$, leading to many Li-ion vacant sites produced in the electrode material. During the discharge process, Li-ions in $Li_2SO_4$ solution could be easily reinserted into the vacant sites, thus obtaining higher discharge specific capacitance.

When using the $K_2SO_4$-, $Na_2SO_4$-, and $(NH_4)_2SO_4$-based electrolytes, the charge process was similar to that in $Li_2SO_4$ solution. Li-ions in spinel $Li_{4+x}Mn_5O_{12}$ material were easily deinserted to form $Li_4Mn_5O_{12}$, leading to Li-ion vacant sites produced in the electrode material. But the discharge process was different. During the discharge process, $M^+$ ($K^+$, $Na^+$, $NH_4^+$) in electrolyte solution was difficult to reinsert into the vacant sites because of their larger sizes. Even if a small amount of cations such as $K^+$, $Na^+$, and $NH_4^+$ were inserted into the $Li_4Mn_5O_{12}$, the stability of the lattice structure

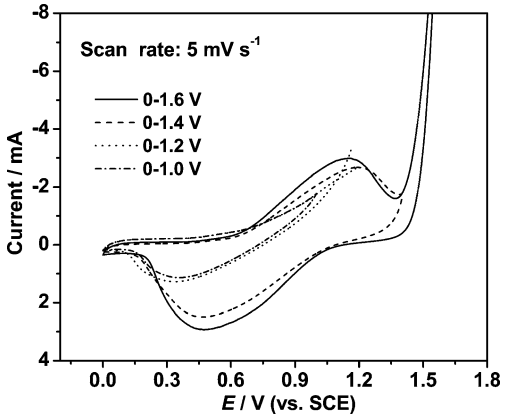


**Fig. 8** CV curves of the $Li_4Mn_5O_{12}$ electrode in various potential limits in 1 M $Li_2SO_4$

would have seriously decreased. Therefore, the capacitive behavior of $Li_4Mn_5O_{12}$/AC capacitor was worse in $Na_2SO_4$, $K_2SO_4$, and $(NH_4)_2SO_4$ solution. In the next experiments, $Li_2SO_4$ solution was chosen as the electrolyte of the $Li_4Mn_5O_{12}$/AC supercapacitor.

*Effect of working voltage*

It is well known that working voltage is one of the predominant factors influencing the energy density of the hybrid pseudocapacitors. To guarantee the electrolyte not to decompose during charge/discharge process in aqueous system, it is important to control a safe potential window without $O_2$ and $H_2$ evolution on the surface of the electrodes. The CV curves of $Li_4Mn_5O_{12}$ and AC in different voltage range in 1 M $Li_2SO_4$ electrolyte solution at scan rate of 5 mV $s^{-1}$ are shown in Figs. 8 and 9, respectively. A sharp peak in Fig. 8 showed that $O_2$ evolution occurred at above 1.4 V (vs. SCE), which is higher than the potential of $O_2$ evolution (1.23 V vs. NHE). So the safe potential window for $Li_4Mn_5O_{12}$ material is controlled between 0 and 1.4 V in 1 mol $l^{-1}$ $Li_2SO_4$.

From the CV curves of $Li_4Mn_5O_{12}$ in the potential range of 0–1.4 V, a pair of broad redox peaks located at about 0.5 and 1.2 V (vs. SCE) are observed. When changing the potential scanning direction, the current direction does not turn around instantly, indicating that the insertion/extraction of Li-ions occurs not only on the surface of the $Li_4Mn_5O_{12}$ powders but also into the inner lattice of the material. The diffusion rate of Li-ions is much lower in the inner lattice of the material than on the surface of the material, so it leads to slower current response.

Figure 9 shows the CV curves of the AC electrode in various potential ranges in 1 mol $l^{-1}$ $Li_2SO_4$ aqueous electrolyte. As shown in the figure, the AC electrode exhibits a rectangular-shaped curve in the potential range of −0.4–1.0 V (vs. SCE) in 1 mol $l^{-1}$ $Li_2SO_4$ aqueous electrolyte, which is the typical characteristic of double-layer capacitance. As clearly shown in Fig. 9, $H_2$ evolution occurred at below −0.8 V vs. SCE. From all the above results, the conclusion can be drawn that no oxygen evolution occurs at $Li_4Mn_5O_{12}$ cathode and no hydrogen evolution occurs at AC anode in the voltage range of 0–1.4 V. So the charge/discharge voltage of the $Li_4Mn_5O_{12}$/AC hybrid pseudocapacitors was controlled between 0 and 1.4 V in 1 M $Li_2SO_4$ electrolyte.

*Effect of scan rate*

In order to get more information on the electrochemical behavior of the $Li_4Mn_5O_{12}$ cathode material, CV characterizations were done at different scan rates of 1, 3, 5, 10, and 20 mV $s^{-1}$ and the results are shown in Fig. 10. From the results of CV, two pairs of redox peaks located at 0.64 and 1.2 V vs. SCE were observed for $Li_4Mn_5O_{12}$ at a scan rate of 1 mV $s^{-1}$, which agrees with the insertion/extraction reaction of $Li_4Mn_5O_{12}$ in the organic electrolyte [22], suggesting that Li-ions could diffuse into the inner lattice of the material.

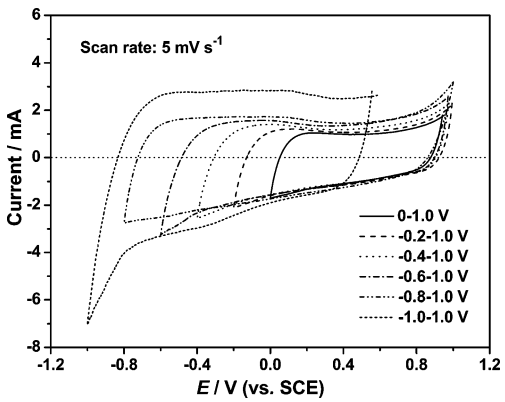


**Fig. 9** CV curves of the AC electrode in various potential limits in 1 M $Li_2SO_4$

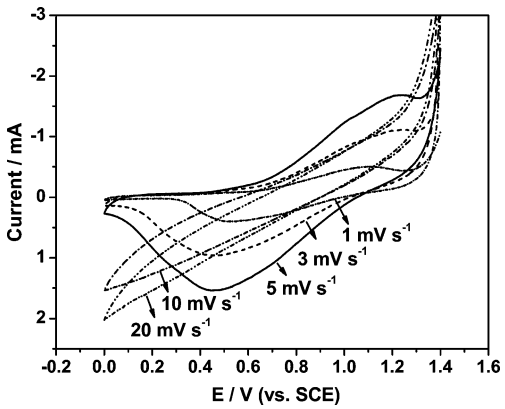


**Fig. 10** CV curves of the $Li_4Mn_5O_{12}$ electrode at different scan rates from 1 to 20 mV $s^{-1}$ in 1 M $Li_2SO_4$

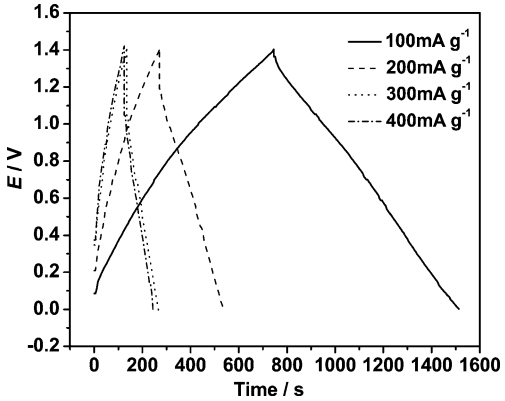


**Fig. 11** Charge/discharge curves of $Li_4Mn_5O_{12}$/1 M $Li_2SO_4$/AC hybrid pseudocapacitor at different current densities

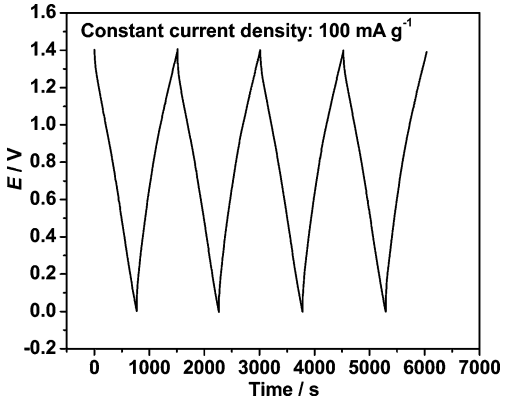


**Fig. 13** Charge/discharge curves of $Li_4Mn_5O_{12}$/1 M $Li_2SO_4$/AC hybrid pseudocapacitor at a current rate of 100 mA/g between 0 and 1.4 V

From the CV recorded at various scan rates, SC values of the single $Li_4Mn_5O_{12}$ electrode are calculated by using the following equation [26]:

$$C = \frac{Q}{2m \cdot \Delta V} \tag{2}$$

where $Q$ refers to the charge integrated from the cathodic sweep and $\Delta V$ and $m$ refers to the difference in the voltage window (here 1.4 V) and weight of the single $Li_4Mn_5O_{12}$ electrode, respectively. The SC values calculated from the CV were 291, 247, and 97 F $g^{-1}$ at scan rates of 1, 5, and 10 mV $s^{-1}$, respectively. The specific capacitance decreased with the increase of the scan rate. The fact can be explained that, when the scan rate increases, the participation of the $Li_4Mn_5O_{12}$ electrode is limited almost to the outer surface and difficult to the inner lattice of $Li_4Mn_5O_{12}$ matrix, leading to a lower specific capacitance with increasing of the scan rate. The active material is utilized insufficiently and faradaic redox reactions occurred almost on the surface of the electrode.

*The effect of charge/discharge current densities*

The rate capability of $Li_4Mn_5O_{12}$/AC hybrid pseudocapacitor was also examined at various current rates from 100 to 400 mA $g^{-1}$. Figures 11 and 12 show the charge/discharge curves and cycling stability of $Li_4Mn_5O_{12}$/1 M $Li_2SO_4$/AC hybrid aqueous pseudocapacitors at different current densities. Apparently, the $Li_4Mn_5O_{12}$/1 M $Li_2SO_4$/AC hybrid pseudocapacitors had the maximum specific capacitance of 43 F $g^{-1}$ and good cycling performance at the current density of 100 mA $g^{-1}$. While at the current density of 400 mA $g^{-1}$ the maximum specific capacitance and cycle ability were very poor. Hence, it is clear that, at a smaller current density, $Li^+$ ions could diffuse into the inner lattice of the material and the redox reactions occurred both on the surface and in the inner lattice of material, and at high current density, the diffusion of $Li^+$ ions was limited almost to the outer surface of electrode and the redox reactions occurred almost on the surface of the electrode, which agrees with the result obtained in cyclic voltammetry test in Fig. 10.

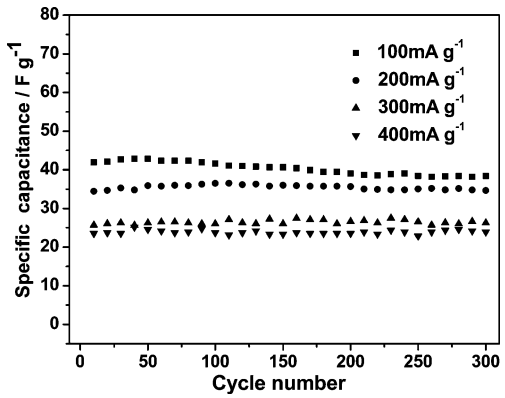


**Fig. 12** Cycling ability of $Li_4Mn_5O_{12}$/1 M $Li_2SO_4$/AC hybrid aqueous pseudocapacitor at different current densities

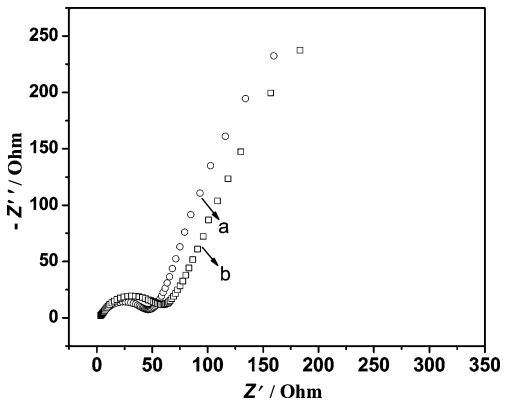


**Fig. 14** Electrochemical impedance spectroscopy plots of $Li_4Mn_5O_{12}$. **a** Before charge/discharge, **b** after 50 cycles between 0 and 1.4 V

The first four cycles of the charge–discharge charge/discharge curves of $Li_4Mn_5O_{12}$/1 M $Li_2SO_4$/AC hybrid pseudocapacitor at a current rate of 100 mA $g^{-1}$ between 0 and 1.4 V are shown in Fig. 13. The E-t behavior as mirror-like during the charge–discharge process meant that a reversible reaction occurred in the electrode materials during the charge and discharge steps, which indicates a typical pseudocapacitance behavior of an ideal supercapacitor and in agreement with the analysis of CV measurement.

*Electrochemical impedance analysis*

Electrochemical impedance spectroscopy of $Li_4Mn_5O_{12}$ before charge/discharge and after 50 cycles between 0 and 1.4 V is shown in Fig. 14. The EIS curves include two parts of a semicircle and a straight line; in low frequency of 100 kHz–0.01 Hz, the semicircle is related to the lithium-intercalation process and in the high frequency of 100–1,000 kHz, a straight line, which keeps at an angle of 70° with the *x*-axis, has a typical capacitive characteristic. As shown in Fig. 14, there is only a little increase in resistance after 50 cycles in comparison with that before charge/discharge. The fact supports the result of XRD analysis before and after cycling and the capacity fading less upon cycling, indicating that $Li_4Mn_5O_{12}$ electrode has a good capacitive behavior and superior cycling performance.

## Conclusion

In this study, we firstly presented hybrid aqueous pseudocapacitors in which the activated carbon (AC) was used as an anode material and a lithium-ion intercalating compound $Li_4Mn_5O_{12}$ as a cathode material in aqueous electrolyte. The research results indicated that calcinations temperature, working voltage, current density; electrolyte species and scan rate had great effect on the electrochemical performance of $Li_4Mn_5O_{12}$ material. The sample annealed at 450 °C for 4 h possesses remarkable electrochemical capacitive behavior and superior cycling performance. $Li_4Mn_5O_{12}$/AC pseudocapacitor exhibited the best electrochemical performance in 1 M $Li_2SO_4$ solution than in other aqueous electrolytes such as 1 mol $l^{-1}$ $K_2SO_4$, $(NH_4)_2SO_4$, and $Na_2SO_4$, which indicate that the charge/discharge mechanism of $Li_4Mn_5O_{12}$/1 M $Li_2SO_4$/AC is associated with the transfer of Li-ions between two electrodes. This hybrid cell exhibited an estimated specific capacity of 43 F $g^{-1}$ based on the total weight of the active electrode materials. $Li_4Mn_5O_{12}$/AC pseudocapacitor also exhibited good cycling performance with the capacity fading rate of 0.0078 F $g^{-1}$ per cycling over 1,000 cycles at the current density of 100 mA $g^{-1}$.

**Acknowledgement** The authors acknowledge the financial support from the National Natural Science Foundation of China (no. 20701029).

## References

1. Amatucci GG, Badway F, Pasquier AD, Zheng T (2001) J Electrochem Soc 148:A930, doi:10.1149/1.1383553
2. Huang BH, Yang P, Zhang BH, Shi QM (2006) J Power Sources 30:560, Chinese
3. Chen F, Li RG, Hou M, Liu L, Wang R, Deng ZH (2005) Electrochim Acta 51:61, doi:10.1016/j.electacta.2005.03.047
4. Pasquier AD, Laforgue A, Simon P (2004) J Power Sources 125:95, doi:10.1016/j.jpowsour.2003.07.015
5. Wang YG, Xia YY (2006) J Electrochem Soc 153:A450, doi:10.1149/1.2140678
6. Wang YG, Lou JY, Wu W, Wang CX, Xia YY (2007) J Electrochem Soc 154:A228, doi:10.1149/1.2432056
7. Wang YG, Lou JY, Wang CX, Xia YY (2006) J Electrochem Soc 153:A1425, doi:10.1149/1.2203772
8. Scrosati B, Panero S, Reale P, Satolli D, Aihara Y (2002) J Power Sources 105:161, doi:10.1016/S0378-7753(01)00935-1
9. Julien CM, Massot M, Zaghib K (2004) J Power Sources 136:72, doi:10.1016/j.jpowsour.2004.05.001
10. Zaghib K, Armand M, Gauthier M (1998) J Electrochem Soc 145:3135, doi:10.1149/1.1838776
11. Zaghib K, Simoneau M, Armand M, Gauthier M (1999) J Power Sources 300:81–82, doi:10.1016/S0378-7753(99)00209-8
12. Tarascon JM, Wang E, Shokoohi FK (1991) J Electrochem Soc 138:2859, doi:10.1149/1.2085330
13. Wen SJ, Richardson TJ, Ma L (1996) J Electrochem Soc 143: L136, doi:10.1149/1.1836902
14. Levi E, Levi MD, Salitra G (1999) Solid State Ionics 126:109, doi:10.1016/S0167-2738(99)00219-2
15. Park YJ, Kim JG, Kim MK (2000) Solid State Ionics 130:203, doi:10.1016/S0167-2738(00)00551-8
16. Liu DQ, He ZZ, Liu XQ (2007) Mater Lett 61:4703, doi:10.1016/j.matlet.2007.03.012
17. Zeng RH, Li WS, Lu DS, Huang QM (2007) J Power Sources 174:592, doi:10.1016/j.jpowsour.2007.06.120
18. Ohzuku T, Kitagawa M, Hirayi T (1990) J Electrochem Soc 137:769, doi:10.1149/1.2086552
19. Thackeray MM, De Kock A, Rossouw MH (1992) J Electrochem Soc 139:363, doi:10.1149/1.2069222
20. Liu D-Q, He Z-Z, Liu X-Q (2007) J Alloy Comp 440:69, doi:10.1016/j.jallcom.2006.09.013
21. Thackeray MM, Mansuetto MF, Johnson CS (1996) J Solid State Chem 125:274, doi:10.1006/jssc.1996.0297
22. Takada T, Hayakawa H, Akiba E, Chakoumakos BC (1997) J Power Sources 68:613, doi:10.1016/S0378-7753(96)02570-0
23. Julien CM, Zaghib K (2004) Electrochim Acta 50:411, doi:10.1016/j.electacta.2004.03.052
24. Singhal A, Skandan G, Amatucci G (2004) J Power Sources 129:38, doi:10.1016/j.jpowsour.2003.11.010
25. Brett A, Deborah J, Roziere J, Burns J, Gary R (1995) Chem Mater 7:2151, doi:10.1021/cm00059a024
26. Hu CC, Wang CC (2002) J. Electrochem Commun 4:554, doi:10.1016/S1388-2481(02)00371-5